

Dual Photochemistry of Benzimidazole

José P. L. Roque, Mário T. S. Rosado, Rui Fausto, and Igor Reva*



Cite This: *J. Org. Chem.* 2023, 88, 2884–2897



Read Online

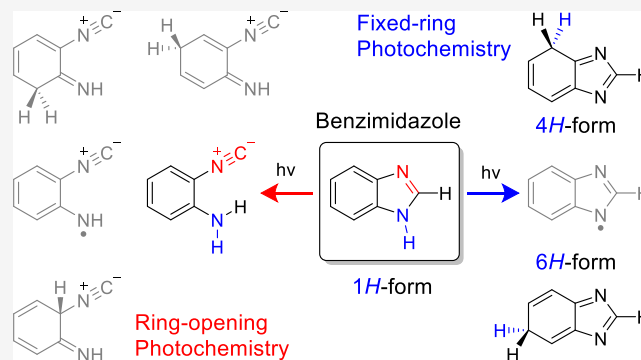
ACCESS |

Metrics & More

Article Recommendations

Supporting Information

ABSTRACT: Monomers of benzimidazole trapped in an argon matrix at 15 K were characterized by vibrational spectroscopy and identified as 1*H*-tautomers exclusively. The photochemistry of matrix-isolated 1*H*-benzimidazole was induced by excitations with a frequency-tunable narrowband UV light and followed spectroscopically. Hitherto unobserved photoproducts were identified as 4*H*- and 6*H*-tautomers. Simultaneously, a family of photoproducts bearing the isocyano moiety was identified. Thereby, the photochemistry of benzimidazole was hypothesized to follow two reaction pathways: the fixed-ring and the ring-opening isomerizations. The former reaction channel results in the cleavage of the NH bond and formation of a benzimidazolyl radical and an H-atom. The latter reaction channel involves the cleavage of the five-membered ring and concomitant shift of the H-atom from the CH bond of the imidazole moiety to the neighboring NH group, leading to 2-isocyanoaniline and subsequently to the isocyanoanilanyl radical. The mechanistic analysis of the observed photochemistry suggests that detached H-atoms, in both cases, recombine with the benzimidazolyl or isocyanoanilanyl radicals, predominantly at the positions with the largest spin density (revealed using the natural bond analysis computations). The photochemistry of benzimidazole therefore occupies an intermediate position between the earlier studied prototype cases of indole and benzoxazole, which exhibit exclusively the fixed-ring and the ring-opening photochemistries, respectively.

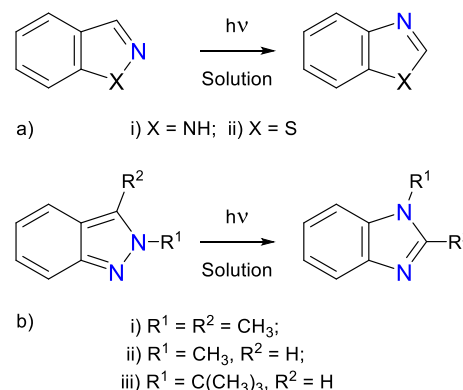


1. INTRODUCTION

Benzimidazole (BzIm) derivatives are the structural bioisosters of naturally occurring purine bases, and the fact that benzimidazole produced biological effects has been recognized long ago.¹ The research on benzimidazole chemistry goes back over a century.^{2–4} Benzimidazole has gained considerable attention in medicinal and pharmaceutical chemistry.⁵ BzIm derivatives interact with the biopolymers of the living system such as proteins, enzymes, and receptors and are frequently used in the development of new therapeutic agents against multiple diseases.^{6–16} The benzimidazole scaffold has also been reported as an organic corrosion inhibitor^{17–22} for different metals in different media and as a multifunctional unit in heteroaromatic molecular systems for optoelectronics, nonlinear optics, photovoltaics, optical sensing, and bioimaging.²³ The structural and spectroscopic features of BzIm are well established. An overview of the most important reports devoted to the characterization of electronic and vibrational spectra of BzIm is provided in the Supporting Information.

Research on the photochemistry of BzIm derivatives has been addressed in solutions (Scheme 1). For instance, Cole *et al.* reported that photolysis of benzimidazole in various solvents with free access to air gives the unsymmetrical dehydromers.²⁴ Similarly, Smitka *et al.* reported that in aqueous solution, the phototransformation of the free BzIm

Scheme 1. Photoreactivity of Benzoannulated Azoles in Solution^{27–32}



leads to dehydromerization,²⁵ while inside cucurbit[8]uril, BzIm undergoes photohydrolysis to yield 2-amino-formani-

Received: October 23, 2022

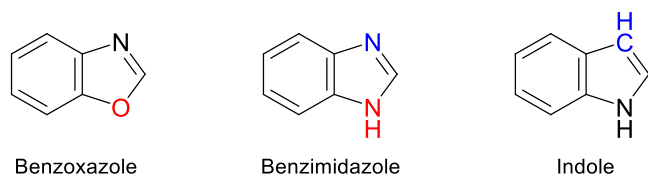
Published: February 16, 2023



lide.²⁵ The photochemistry of 2-iodo-substituted BzIm yields aromatic ring-fused benzimidazoles *via* substitutions of the benzimidazol-2-yl radical.²⁶ The latter finding agrees with the report of Cole *et al.*,²⁴ who found that 2-alkylbenzimidazoles do not give dimers but produce a mixture of acyl derivatives. N1-protonated benzopyrazoles^{27,28} and benzisothiazoles were found to undergo isomerizations to the corresponding benzimidazoles and benzothiazoles (Scheme 1a).²⁹ Similar transformations occur with 2-alkyl-indazoles which undergo photoisomerization to 1-alkyl-benzimidazoles (Scheme 1b).^{30–32} Interestingly, photoisomerizations opposite to those shown in Scheme 1 have not been reported. Although some reports about the photochemistry of benzimidazole in condensed media have already been published,^{24–26,33} to the best of our knowledge, there are no reports on its photoinduced unimolecular transformations.

Recently, we and others have successfully employed the matrix-isolation technique to study the photochemistry of monomeric benzoannulated azoles.³⁴ In the context of this work, it is important to highlight the photochemistry of benzoxazole (BzOx) and indole (see Chart 1).

Chart 1. Molecular Structures of Benzoxazole, Benzimidazole, and Indole

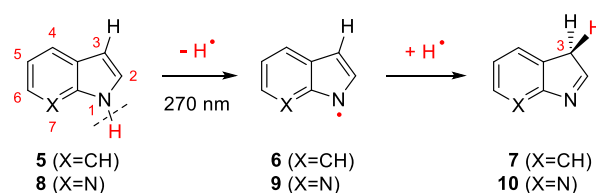


Despite their structural similarity with BzIm, the photochemistry of monomeric BzOx and of monomeric indole was found to be rather different. For example, the photochemistry of BzOx **1** is initiated by the cleavage of the CO bond ($\lambda = 233$ nm), leading to quantitative formation of isomeric 2-isocyanophenol **2** (Scheme 2). Upon irradiation at longer wavelengths ($\lambda = 270$ nm), the open-ring 2-isocyanophenol photoisomerizes back to BzOx or undergoes photoinduced cleavage of the OH bond, leading to the formation of 2-isocyano-phenoxy radical **3** and an H atom (also a radical). The subsequent recombination of the radical pair at different positions of **3** leads, among other products, to isocyano-substituted cyclohexadienone **4** (Scheme 2).

In the case of indole (or its isomeric 7-azaindole), the photoinduced ring-opening reactions were not observed. Instead, the photochemical reactions involved the cleavage of the NH bond. The indolyl radical **6** or 7-azaindolyl radical **9** (along with the photodetached H-atom) were found to play a crucial role in the formation of prototropic 3H-tautomers of indole (**7**)³⁶ or azaindole (**10**)³⁷ (Scheme 3).

One can expect that the photochemistry of monomeric BzIm might bear similarities with that of either BzOx or indole,

Scheme 3. Photoinduced Reactivity of Monomeric Indole and 7-Azaindole^{36,37,a}



^aNumbering of heavy atoms of the starting compounds and ring position 3 of the photoproducts are shown in red.

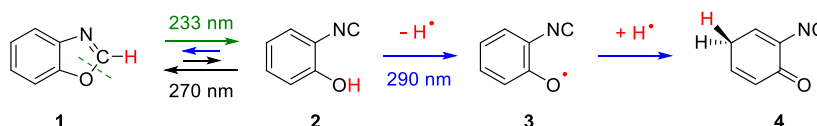
or both, making it unpredictable and challenging. Herein, we report on the photochemistry of monomeric benzimidazole isolated in a low-temperature Ar matrix, by employing infrared (IR) spectroscopy to characterize its photoproducts and density functional theory (DFT) computations to support the mechanistic interpretations.

2. RESULTS AND DISCUSSION

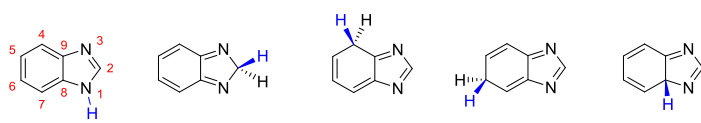
2.1. Structural and Vibrational Characterization of Benzimidazole. Five unique prototropic tautomers of BzIm were found as minima on its potential energy surface (PES). According to the computations, the 1H-BzIm (1H-benzimidazole) is the most stable by more than 130 kJ mol⁻¹ (see Table 1). The aromatic arrangement of the π electrons in the two fused rings results in an increased stability of 1H-BzIm compared to that of the remaining forms. As discussed in the Supporting Information, the structural and spectroscopic characterization of the 1H-form of monomeric BzIm is vast and comprehensive.^{38–41} However, there is virtually no data available in the literature regarding other tautomeric forms of parent BzIm. The exceptions only briefly mention tautomerism of BzIm within the imidazole ring involving the N1, C2, and N3 atoms.^{42,43}

Considering the relative stability of BzIm tautomers (Table 1), 1H-BzIm should dominate in the gas phase, and it should be the only form trapped from gas into a cryogenic matrix. Indeed, the three strongest bands found in the IR spectrum of BzIm isolated in an argon matrix (15 K) at 3509, 742/740, and 459/449 cm⁻¹ are assigned to characteristic modes of the 1H-form, namely, to the NH stretching $\nu(\text{NH})$, the in-phase CH out-of-plane bending $\gamma_d(\text{CH})$, and the NH out-of-plane bending $\gamma(\text{NH})$, respectively (see Figure 1 and Tables S1 and S2). The overall IR spectrum of BzIm isolated in solid argon is in agreement with previously published spectroscopic data.^{38,44} Moreover, the experimental IR spectrum is very well reproduced by the theoretical spectrum of 1H-BzIm (see Figure 1 and Tables S1 and S2). The exception is a medium-intensity band found at 944 cm⁻¹ (Figure 1a), not predicted by calculations in the harmonic approximation. This band should be assigned to the first overtone of the NH out-of-plane bending mode [$2\gamma(\text{NH})$], for which the anharmonic

Scheme 2. Photoinduced Reactivity of Monomeric Benzoxazole^{35,a}



^aNote color codes for the irradiations at different wavelengths.

Table 1. Structures, Relative Electronics (ΔE), and Gibbs Free (ΔG) Energies (at 298.15 K) Computed for the Prototropic Tautomers of Benzimidazole^a


Tautomer ^b	1H (3H)	2H	4H (7H)	6H (5H)	8H (9H)
ΔE	0.0	134.5	144.5	137.5	184.7
ΔG	0.0	130.3	138.3	132.1	180.8

^aComputed at the B97-1/def2-TZVP level of theory. Absolute computed energies (in Hartree) for the 1H-tautomer are $E_h = -379.89895687$ and $G = -379.8122136$. All relative energies (in kJ mol^{-1}) are with respect to 1H-BzIm. Numbering of heavy atoms is shown in red for the 1H-tautomer. Numbering of all atoms (including H atoms) is shown in Figure S1. The labile H-atom is shown in blue. ^bThe names of symmetry-equivalent tautomeric forms are shown in parentheses.

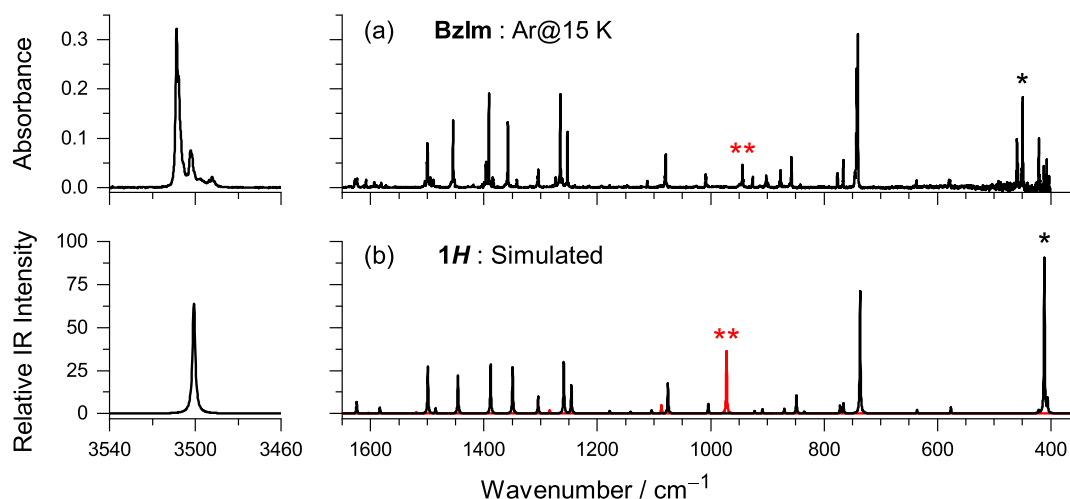


Figure 1. (a) Experimental IR spectrum of benzimidazole monomers isolated in an argon matrix at 15 K. (b) Black trace—simulated IR spectrum of 1H-BzIm computed at the B97-1/def2-TZVP level of theory in harmonic approximation. See the Experimental Section for details of simulation. See Figure S2 for the linear fit and determination of the scaling factor. Red trace—simulated spectrum of the first overtones (computed anharmonic frequencies unscaled). The bands marked with one and two asterisks (in both frames) are, respectively, assigned to the fundamental and the first overtone transitions of the NH out-of-plane bending $\gamma(\text{NH})$ mode.

calculation predicts a transition at 972 cm^{-1} with an IR intensity of 36.4 km mol^{-1} (Figure 1b). The observation in the IR spectra of similar overtone bands was previously reported for matrix-isolated indole³⁶ [$2\gamma(\text{NH}) = 804 \text{ cm}^{-1}$] and 7-azaindole³⁷ [$2\gamma(\text{NH}) = 927 \text{ cm}^{-1}$] and should be a common trend for aromatic molecules containing the NH group.

2.2. Fixed-Ring H-Scrambling Photochemistry of 1H-Benzimidazole. The lowest energy spin-allowed electronic transition of 1H-BzIm has been assigned as a $\pi^* \leftarrow \pi$ transition, with origin at 36021.38 cm^{-1} ($\sim 277.61 \text{ nm}$) in the gas phase.⁴¹ Initial irradiations of matrix-isolated benzimidazole were carried out at longer wavelengths, at 300 and 290 nm, but did not lead to any change in the IR spectrum. After narrow-band (fwhm = 0.2 cm^{-1}) irradiations at $\lambda = 280 \text{ nm}$, a trace amount of the 1H-BzIm form was consumed, and the transformation was barely discernible, but upon irradiations at $\lambda = 277 \text{ nm}$, i.e., near the electronic origin of BzIm,^{40–42,45–47} it started to react more extensively ($\sim 15\%$ consumed in 140 s). Concomitantly, two sets of new bands emerged in the IR fingerprint region and could be assigned to two different products, A and B, because they exhibited different kinetic patterns of formation. These two species were found to be persistent under matrix-isolation conditions on the timescale of our experiments (hours). Two non-overlapping bands, characteristic of the new photoproducts, were found in the

$1565\text{--}1540 \text{ cm}^{-1}$ spectral range: at 1560 cm^{-1} , assigned to product A and at 1547 cm^{-1} , assigned to product B (Figure 2). Upon a few minutes of irradiation at $\lambda = 277 \text{ nm}$, both the amount of consumed 1H-BzIm and the amounts of products A and B reach a plateau, suggesting the existence of a photo-stationary equilibrium among the three structures (see spectra in the blue palette in Figure 2). Upon subsequent irradiation of the matrix at $\lambda = 248 \text{ nm}$ (that corresponds to the second excited $\pi\text{--}\pi^*$ singlet state of 1H-BzIm, which was reported to have an energy of 5.0 eV in aqueous solution),⁴⁸ the previous photo-stationary state is perturbed. Irradiations at 248 nm not only enhance the consumption of the 1H-form but also change the ratio of formation of the two photoproducts (A/B) (see Figure 2). Additionally, it was found that by irradiating freshly deposited matrices of BzIm at $\lambda = 277 \text{ nm}$, the A/B ratio would be close to unity (47:53), whereas for initial irradiations at $\lambda = 260 \text{ nm}$, the ratio shifted in favor of A (A/B = 78:22).

The remaining bands of products A and B were also distinguished based on their kinetics of growth upon ultraviolet irradiations. Subsequently, each set of bands was compared with putative photoproducts of 1H-BzIm, and a close agreement was found between the IR spectrum assigned to product A and that computed for 4H-benzo[d]imidazole (4H-BzIm), as well as between the IR spectrum assigned to product B and that computed for the 6H-benzo[d]imidazole

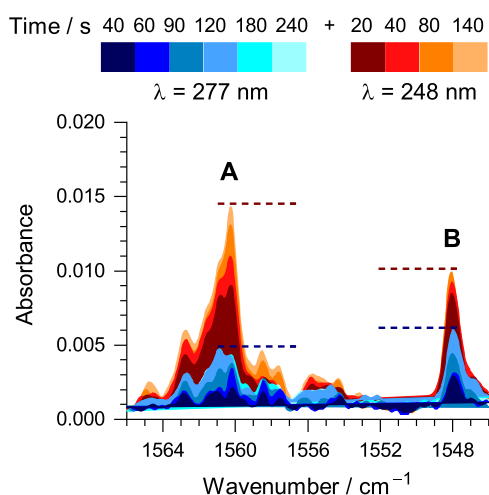


Figure 2. Changes of the IR spectra of BzIm isolated in an Ar matrix at 15 K during a sequence of irradiations, initially at $\lambda = 277$ nm (blue palette) and subsequently at $\lambda = 248$ nm (brown palette). The bands with maxima near 1560 and 1548 cm^{-1} were assigned to species A and B, respectively, photogenerated from 1*H*-BzIm. The dashed lines represent the peak intensities of A and B corresponding to two photostationary states.

(6*H*-BzIm)⁴⁹ (Figure 3). The bands of products A and B, shown in Figure 2, were assigned to the vibrations of double bonds. The band of A centered at 1560 cm^{-1} was assigned to the $[\nu(\text{C7}=\text{C8}) + \nu(\text{C5}=\text{C6})]$ mode of 4*H*-BzIm, predicted to be its third most intense IR band (80 km mol^{-1}). The band of B centered at 1548 cm^{-1} was assigned to the $[\nu(\text{C5}=\text{C4}) - \nu(\text{C9}=\text{N3}) + \nu(\text{C2}=\text{N1})]$ mode of 6*H*-BzIm, predicted to be its second most intense IR band (56 km mol^{-1}). Other characteristic bands of the newly identified benzimidazole tautomers were found at 1665 (6*H*-) and 1657 cm^{-1} (4*H*-) due to C7=C8 stretching modes, with computed counterparts at 1672 and 1663 cm^{-1} , respectively. Notice that 1*H*-BzIm has its highest-frequency $\nu(\text{CC})$ stretching mode at a much lower wavenumber (1627 cm^{-1}). The characteristic bands due to the

methylene scissoring modes $\delta(\text{CH}_2)$ of the new tautomers were found at 1367 (6*H*-) and 1360 cm^{-1} (4*H*-), with nearly the same computed frequencies. The observed frequencies are in close agreement with those of previously identified $\delta(\text{CH}_2)$ modes of two photogenerated thione isomers of matrix-isolated thiophenol at 1363 and 1389 cm^{-1} .⁵⁰ A detailed characterization of the IR spectra of 4*H*-BzIm and 6*H*-BzIm is provided for the first time in Tables S3 and S4, respectively. It is particularly noteworthy that for each of the two new tautomers, all the vibrational modes in the 1700–600 cm^{-1} range with predicted IR intensities over 10 km mol^{-1} (non-overlapping with 1*H*-BzIm) have been identified in the experiment.

Finally, it is also worth mentioning that there was no evidence of the formation of 2*H*-BzIm throughout the experiments. For example, the absence of a photoproduct band around 750 cm^{-1} , where the most intense IR mode of 2*H*-BzIm is predicted, in a spectral region free of bands of either the precursor 1*H*-BzIm or photoproducts 4*H*-BzIm and 6*H*-BzIm suggests that 2*H*-BzIm is not a product of benzimidazole photochemistry in an argon matrix.

2.3. Fixed-Ring Photochemistry of 4*H*- and 6*H*-Tautomers. Tautomers 4*H*- and 6*H*- of benzimidazole contain localized and conjugated double bonds, unlike the aromatic 1*H*-form, and should therefore possess electronic transitions at longer wavelengths because conjugation of double bonds leads to reduction of the band gap for $\pi^* \leftarrow \pi$ transitions. In fact, time-dependent DFT (TD-DFT) calculations reveal that 4*H*- and 6*H*-forms should absorb light at wavelengths longer than 1*H*-form absorbs. Intense electronic $\pi^* \leftarrow \pi$ transitions were predicted at 335 nm for 6*H*-BzIm and at 349 nm for 4*H*-BzIm, at much longer wavelengths than the corresponding computed lowest-energy transition of 1*H*-BzIm at 247 nm (see Figure S3 and Table S5).

The initial UV irradiations of 1*H*-BzIm were carried out using different laser wavelengths yet always in the $\lambda < 280$ nm range, where the 1*H*-tautomer absorbs UV light. Aiming at further photochemical transformations of 4*H*- and 6*H*-forms, generated herein for the first time, the matrix was subjected to

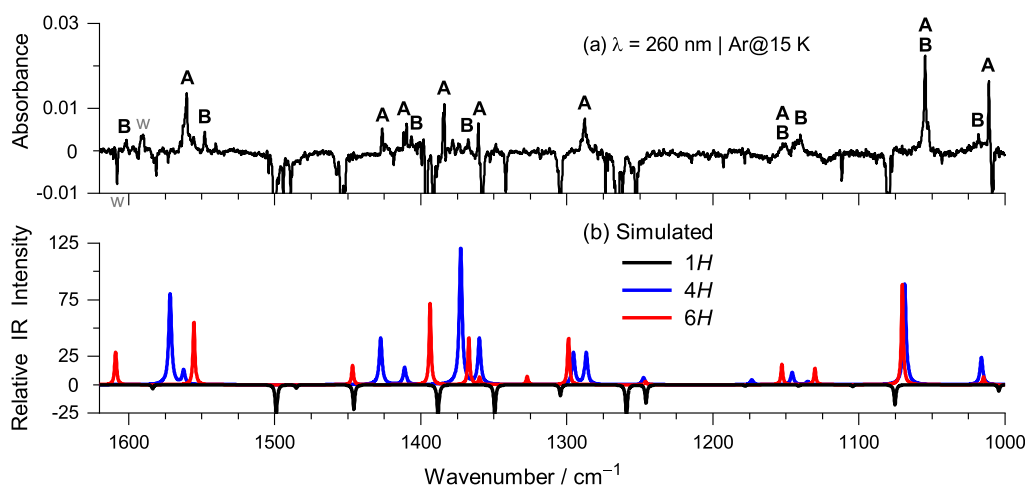


Figure 3. (a) Experimental difference IR spectrum showing changes upon UV irradiation at $\lambda = 260$ nm of BzIm isolated in an Ar matrix at 15 K. The downward bands are due to consumed species assigned to 1*H*-BzIm (truncated), and the upward bands are due to the photoproducted species A and B, distinguished based on further photo-transformations (see discussion below). The bands near 1600 cm^{-1} marked with w (dimmed) correspond to matrix-isolated monomeric water. (b) Simulated IR spectra of 1*H*-BzIm (black line), 4*H*-BzIm (blue line), and 6*H*-BzIm (red line) computed at the B97-1/def2-TZVP level of theory. The theoretical vibrational frequencies were scaled by 0.983, and the IR intensity of 1*H*-BzIm was multiplied by -1 .

a series of narrow-band irradiations at longer wavelengths, where 1*H*-BzIm does not absorb. The initial wavelength was set at $\lambda = 400$ nm, and then, the wavelengths of subsequent irradiations were decreased in steps of 10 nm. Upon the irradiation at 380 nm, the IR intensity of the bands assigned to 4*H*-BzIm decreased, and the IR intensity of the bands assigned to 6*H*-BzIm simultaneously increased. A careful analysis shows that 1*H*- was also partially repopulated at the cost of 4*H*-BzIm, which is evidence that indeed, species **A** and **B** are isomers of 1*H*-BzIm, rather than its decomposition products. Later, it was found that upon irradiation at $\lambda = 260$ nm, the 4*H*- tautomer would be repopulated, and this cycle could be repeated multiple times. The consumption/repopulation cycle of 4*H*- was repeated, while reducing the wavelength of irradiation used to consume 4*H*- (below 380 nm). The most efficient consumption of 4*H*- occurred upon irradiations at $\lambda = 330$ nm, where a 30 s irradiation was enough to totally consume it (see Figure 4).

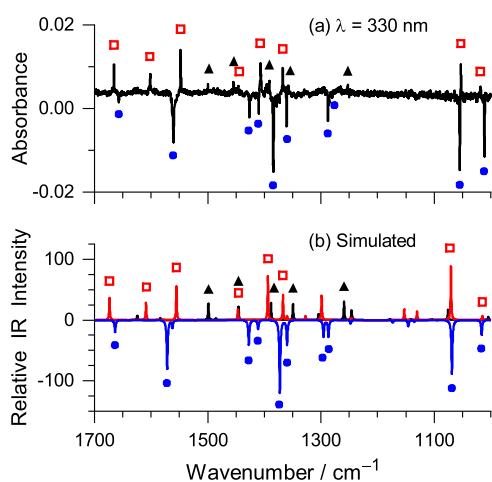


Figure 4. (a) Experimental difference IR spectrum showing changes upon UV irradiation at $\lambda = 330$ nm, subsequent to the initial irradiation at $\lambda = 260$ nm of BzIm isolated in an Ar matrix at 15 K. The downward bands are due to consumed 4*H*-BzIm (blue circles); the upward bands are due to photoproducted 6*H*-BzIm (red squares) and 1*H*-BzIm (black triangles). (b) Simulated IR spectra of 1*H*-BzIm (black line), 4*H*-BzIm (blue line), and 6*H*-BzIm (red line) computed at the B97-1/def2-TZVP level. The theoretical vibrational frequencies were scaled by 0.983, and the IR intensity of 4*H*-BzIm was multiplied by -1 .

Upon total consumption of 4*H*- and enrichment of the matrix with 6*H*-, a search was conducted to find out which wavelengths allow its selective consumption. Narrow-band irradiation at $\lambda = 283$ nm, i.e., at an energy slightly below that of the electronic origin of 1*H*-, led to the consumption of 6*H*- and major recovery of 1*H*-. Importantly, signs of the formation of 4*H*- were also found (see Figure S4). These results are in line with the TD-DFT computations, which predict 6*H*- to have an allowed transition ($f = 0.0820$) at 260 nm, a wavelength longer than that of the first spin-allowed transition of 1*H*- computed at 247 nm.

2.4. Ring-Opening Photochemistry of the 1*H*-Benzimidazole Tautomer. Upon the initial irradiations of matrix-isolated BzIm at wavelengths below 280 nm, a set of new low-intensity bands was found in the 2200–2000 cm^{-1} frequency range. This region is characteristic of stretching vibrations of molecular fragments containing either triple bonds or

cumulated double bonds (e.g., nitrile, isonitrile, ketene, and allene, among others) and therefore could not be ascribed to either 4*H*-BzIm or 6*H*-BzIm. The multiplet feature shown in Figure 5 appears during the first instants of irradiation (1 min

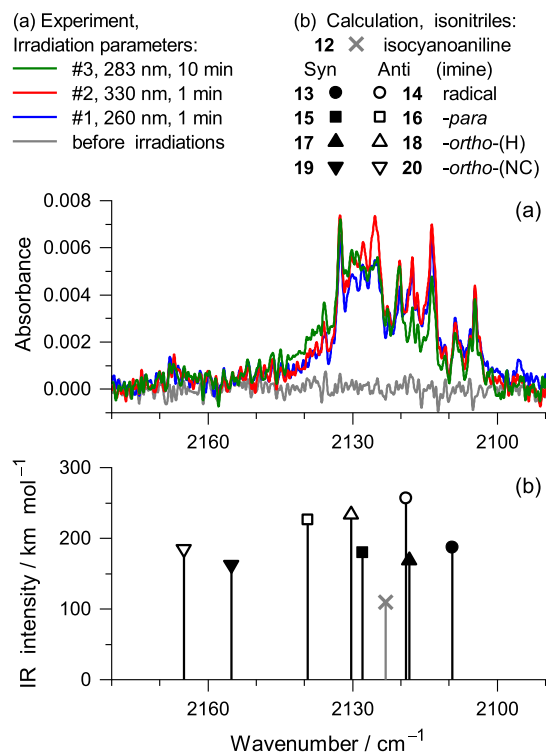
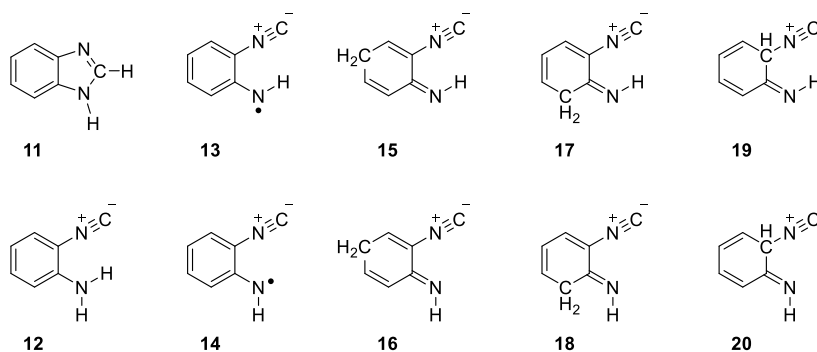


Figure 5. (a) Characteristic fragment of the IR spectra of benzimidazole isolated in an Ar matrix at 15 K: before irradiations (gray line) and after UV irradiations at 260 nm (blue line), 330 nm (red line), and 283 nm (green line). (b) B97-1/def2-TZVP-computed harmonic wavenumbers and IR intensities for putative isocyano photoproducts. Respective structures are shown in Chart 2. The computed frequencies were scaled as discussed in the Computational Section.

at 260 nm), and from that point on, it remains always present, after any UV irradiation, contrasting with the kinetics of growth and disappearance of isomers 4*H*-BzIm and 6*H*-BzIm, both of which ultimately disappear upon irradiations at 283 nm.

In the context of the current investigation, it should be noticed that isocyano ($-\text{N}\equiv\text{C}$) compounds could be produced upon cleavage of the N1–C2 bond (and simultaneous cleavage of the C2–H bond). The NC stretching mode of the $-\text{N}\equiv\text{C}$ group has been found for other compounds, either matrix-isolated or in solutions, to give rise to sharp IR bands in the 2160–2100 cm^{-1} range.^{51–54} The band shown in Figure 5, on the other hand, appears broad and with a complex multiplet structure centered around 2120 cm^{-1} (spanning about 40 cm^{-1} , see Figure 5), suggesting the contribution of multiple isocyano species. The $\nu(-\text{N}\equiv\text{C})$ stretching mode is characterized by intrinsically high absorption coefficients in IR (hundreds of km mol^{-1}).^{35,54,55} Yet the components of the broad multiplet band around 2120 cm^{-1} were found with low peak IR absorbance (between 4×10^{-3} and 8×10^{-3}). These factors make the unequivocal assignment of the photoproducts responsible for such absorptions difficult because the IR bands due to other

Chart 2. Structures of Benzimidazole and its Isonitrile (Isoicyano) Derivatives



vibrations (of the photoproducts carrying the isocyno group) would have too low intensities to be detected. Nonetheless, as justified below, we propose that 2-isocyananiline (ICA) **12** (see Chart 2) should be formed, upon concerted cleavage of the N1–C2 bond in 1*H*-BzIm **11** and [1,2]H-shift from the C2–H group to the N1 atom. The changes in the NH stretching range of the spectra, consistent with formation of ICA, are presented in Figure 6.

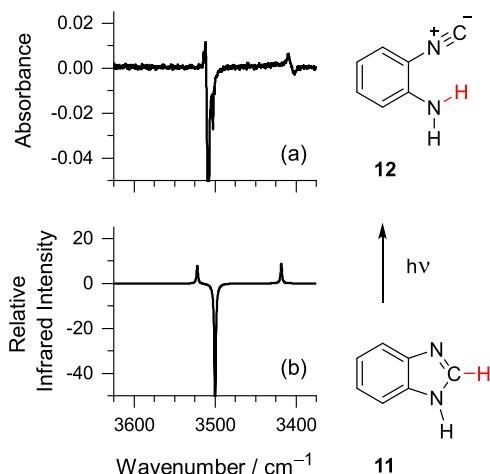


Figure 6. (a) Changes in the spectrum of matrix-isolated BzIm after 2 min of irradiation at $\lambda = 248$ nm. The negative (truncated) band is due to the BzIm precursor. Positive bands are due to the photoproduct. (b) Simulated IR difference spectrum computed at the B97-1/def2-TZVP level. The positive bands are due to ICA **12** (note that computed IR intensities of **12** were scaled by 0.25, which makes it clear that conversion from **11** to **12** is not quantitative). The negative (computed IR intensity scaled by -1 , truncated) band is due to 1*H*-BzIm **11**. All computed frequencies in this range were scaled by 0.955.

The new bands appearing at 3511 and 3409 cm^{-1} (Figure 6a) have a good match with the theoretically predicted bands of ICA at 3522 and 3418 cm^{-1} (Figure 6b), ascribed to the antisymmetric and symmetric NH_2 stretching modes of ICA, respectively. The absolute positions of these bands in the IR spectrum, and separation of an approximately 100 cm^{-1} , are in good agreement with the respective values reported for the NH stretching modes of the parent aniline^{56–59} and 2-cyanoaniline⁶⁰ in the gas-phase jet-cooled molecular beam and in cryogenic matrix. Note that conversion of 1*H*-BzIm **11** to ICA **12** can be only partial because it occurs simultaneously with the conversion of 1*H*-BzIm into its tautomers 4*H*-BzIm and

6*H*-BzIm, as discussed earlier in Sections 2.2 and 2.3. This is in accordance with the estimate that around 20% of consumed **11** is converted to **12**. The spectral manifestations of ICA in the fingerprint range are difficult to confirm or deny because this spectral range is congested, and the bands of **12** are predicted at close positions as the bands of precursor **11**. The non-accumulation of **12** in the cryogenic matrix can be explained by the fact that the wavelengths required to induce the UV reactions of **11** (277 nm or shorter) must be simultaneously acting on photogenerated **12**, leading to its subsequent phototransformations (see below). The $\nu(-\text{N}\equiv\text{C})$ stretching mode in ICA is computed at 2123 cm^{-1} (109.6 km mol^{-1} , see Figure 5b), near the experimental value reported for phenylisocyanide at 2125 cm^{-1} .⁶¹

We propose that N–H homolytic cleavage in the amino group of **12** shall give rise to the 2-isocyananiliny radical (**13**, **14**, see Chart 2) and an H atom. Note that two radical isomers (*syn* **13** or *anti* **14**), differing by the orientation of the imino group relative to the isocyno group, could be produced upon the N–H bond cleavage in the amino group. Furthermore, recombination of the H atom with **13** or **14** at para or ortho positions with respect to the imino group⁶² shall give rise to three pairs of *syn* or *anti* isomers (see Chart 2), namely, 2-isocyanocyclohexa-2,5-dienimine (*syn* **15** or *anti* **16**), 2-isocyanocyclohexa-2,4-dienimine (*syn* **17** or *anti* **18**), or 6-isocyanocyclohexa-2,4-dienimine (*syn* **19** or *anti* **20**). This hypothesis is in line with the fact that the band observed at 2140–2100 cm^{-1} shows overlapping absorptions of multiple species. Interestingly, the computed IR frequencies of the $\nu(-\text{N}\equiv\text{C})$ modes for the mentioned candidate photoproducts span from 2165 to 2109 cm^{-1} , corroborating the proposed interpretation. Further insights into the mechanism underlying such reactivity are discussed below.

2.5. Mechanistic Analysis of the Fixed-Ring Photochemistry. The pivotal role of the optically dark $\sigma^* \leftarrow \pi$ excited states in the photochemistry of heteroaromatic compounds containing endocyclic NH groups, such as pyrrole, imidazole, or indole, was recognized theoretically and presented as a new paradigm in photochemistry of aromatic biomolecules by Sobolewski *et al.*⁶³ The $\sigma^* \leftarrow \pi$ states are characterized by a repulsive PES along the NH bond stretching and might lead to the homolytic cleavage of the hydrogen atom from the NH bond. Predictions of Sobolewski and co-authors received experimental verification by photofragment translational spectroscopy, *via* the detection of fast detached hydrogen atoms from UV-irradiated azoles in the gas phase.^{64–67} Experimental and theoretical investigations have also reported the importance of $\sigma^* \leftarrow \pi$ states in the

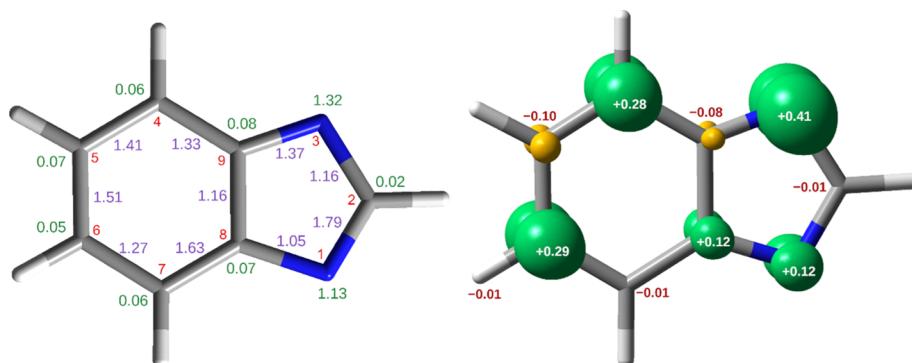


Figure 7. Left: structure of the benzimidazolyl radical optimized at the UB97-1/def2-TZVP level showing NRT bond orders (purple, only values higher than 1.0 included) and non-bonding orbital populations (green, only values higher than 0.02 included). Numbering of the heavy atoms is shown in red. Right: spin density surface (isovalue ± 0.01 e) for the benzimidazolyl radical. Green color stands for alpha spin density (“+” sign) and yellow for beta spin (“-” sign). Element colors: H—white; C—gray; and N—blue. The values near the heavy atoms correspond to the calculated atomic natural spin density values.

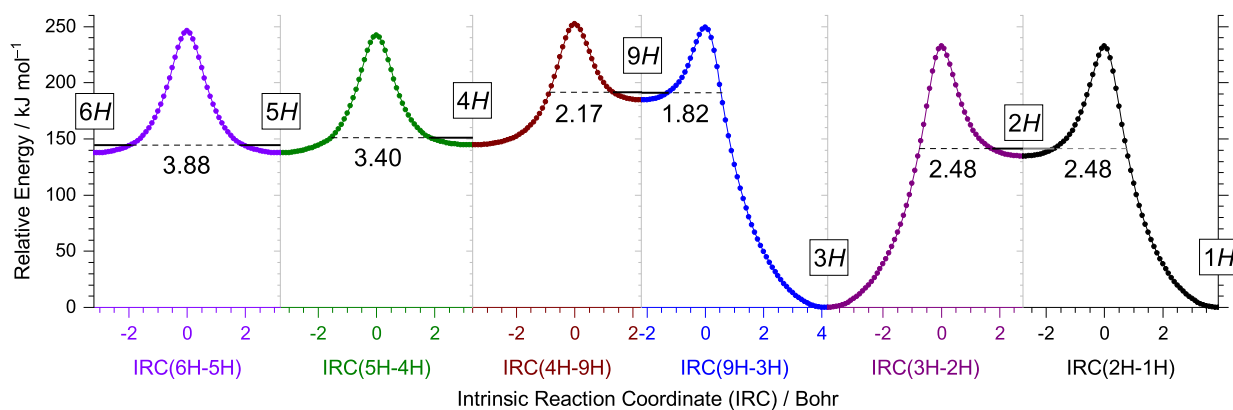


Figure 8. Potential energy profiles along the intrinsic reaction coordinates (IRCs) for the *H*-shifts between neighboring heavy atoms in the benzimidazole system computed at the B97-1/def2-TZVP level in non-mass-weighted (Cartesian) coordinates. The absolute electronic energy of the 1*H*-BzIm tautomer was taken as the relative zero. Horizontal solid lines represent the zero-point vibrational energy (ZPVE) levels of the higher-energy tautomer in each pair. Dashed lines represent the barrier widths for H-atom tunneling at the ZPVE level. See Table 1 for the graphical representation of the prototropic tautomers and for their energies.

photochemistry of imidazole,^{63,68–71} which, in fact, is the five-membered ring contained in benzimidazole. Concomitantly, for several aromatic azoles isolated in cryogenic matrices, the formation of the corresponding radicals upon UV-induced detachment of the H-atom has been observed.^{72–74} Interestingly, the formation of unusual tautomers for these matrix-isolated molecules does not require the presence of intramolecular H-bonds but instead results from the recombination of the released H-atom and its complementary radical in positions far from those where the initial dissociation took place.^{36,37} Such a process is facilitated in cryogenic matrices due to the confinement of both fragments constituting the radical pair produced in the same matrix cavity (cage effect)⁷⁵ and has been coined by Sobolewski *et al.* as photoinduced dissociation association (PIDA).^{75,76}

On the basis of the aforementioned, it is likely that the photochemistry reported in Sections 2.2 and 2.3, involving a dynamic photoequilibrium among three benzimidazole tautomers (1*H*-, 4*H*-, and 6*H*-), occurs *via* the PIDA mechanism and that the benzimidazolyl radical (Figure 7), formed upon homolytic cleavage of the NH bond in 1*H*-BzIm, plays a key role in such processes. This reactivity will from now on be referred to in this work as *fixed-ring photochemistry*. The benzimidazolyl radical contains an unpaired alpha electron

(doublet multiplicity) and belongs to the C_s symmetry point group. There is no principal axis of rotation intercepting the C2H bond (Figure 7, left). According to the natural resonance theory (NRT) analysis of the benzimidazolyl radical, C2N3 becomes essentially a single bond (NRT bond order of 1.16), whereas the N1C2 bond in the benzimidazolyl radical takes a character close to that of a double bond (NRT bond order of 1.79). Similar NRT bond orders, essentially a double N1C2 bond and a single C2C3 bond, were found for the indolyl and 7-azaindolyl radicals.^{36,37} Natural bond orbital (NBO) analysis of the benzimidazolyl wavefunction showed that most of the unpaired alpha spin density is centered around the N3 (+0.41 e), C6 (+0.29 e), C4 (+0.28 e), N1 (+0.12 e), and C8 (+0.12 e) atoms (see Figure 7, right). According to NRT analysis (Figure S5), which decomposes a wavefunction into the Lewis structure contributors, the resonance structures with the largest weights have the radical center located mainly on the C4 (14.2%), N3 (12.6%), C6 (7.0%), and N1 (4.1%) atoms. It is likely that initially detached H-atoms recombine with the corresponding benzimidazolyl radical at those positions with higher spin density. Precisely such type of reactivity was experimentally observed for indole³⁶ and a series of substituted indoles,^{37,73,74} where the new 3*H*-tautomers were experimentally detected, in accordance with the largest predicted spin

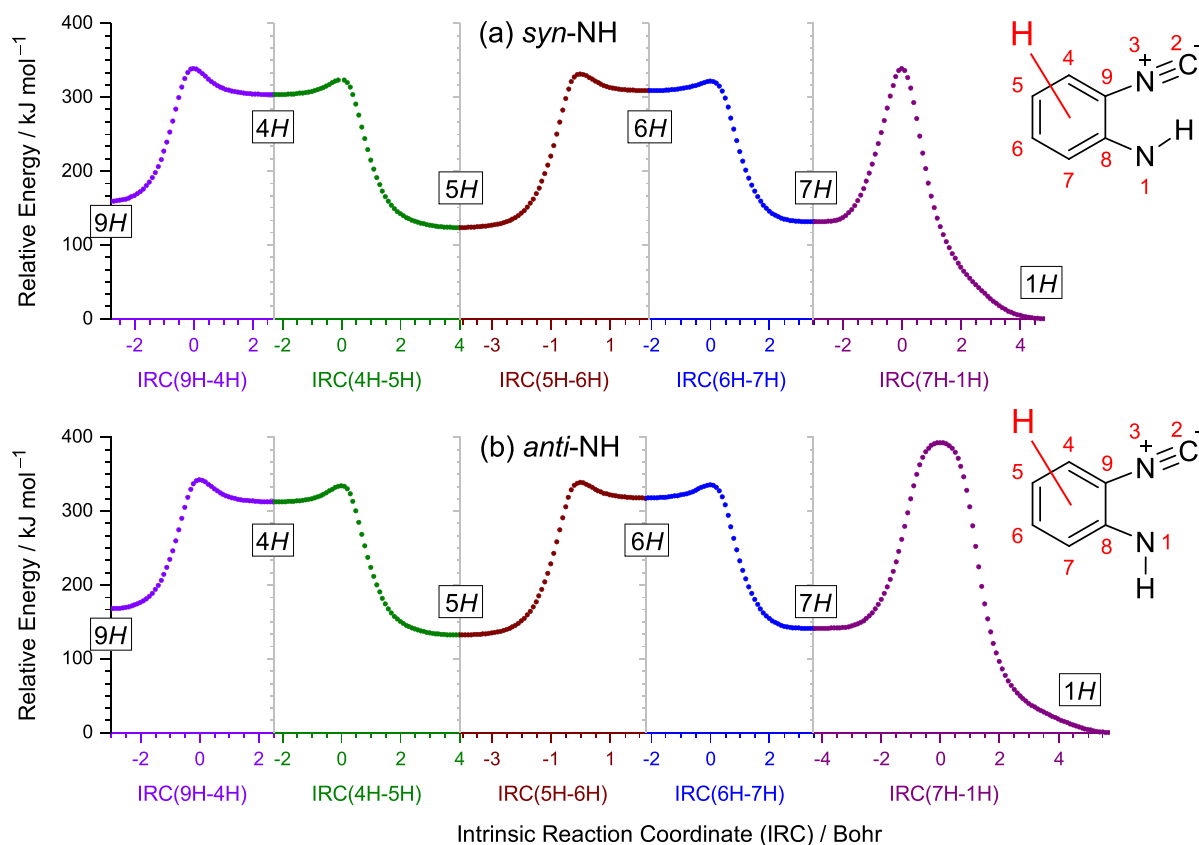


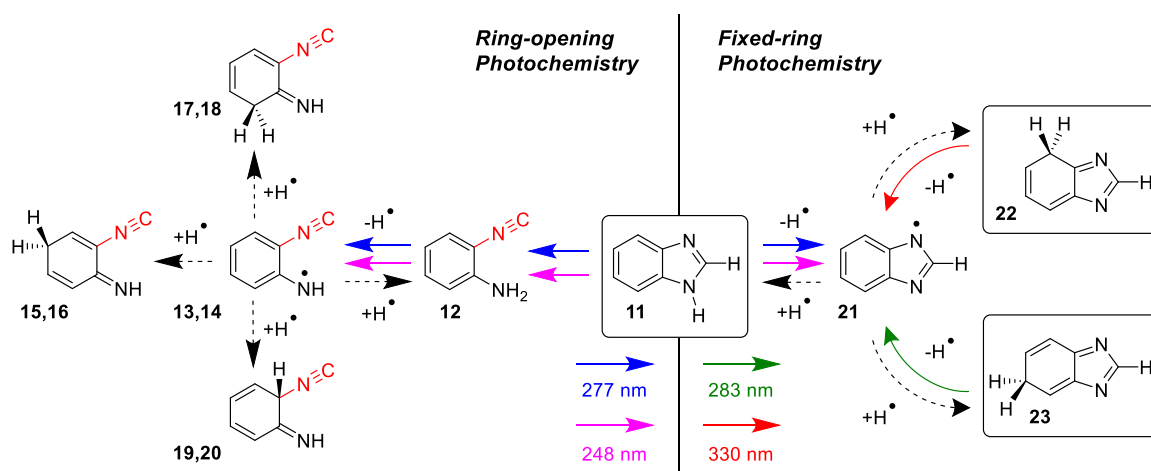
Figure 9. IRC profiles for the H-shifts around the six-membered ring (the migrating H atom is marked in red) computed at the B97-1/def2-TZVP level in non-mass-weighted (Cartesian) coordinates. The energy of 1H was set as the relative zero. The *syn*-NH and *anti*-NH imino isomers of 2-isocyanoaniline are shown near the IRC profiles, along with the atom numbering. The ring positions 4-, 6-, 7-, and 9- correspond to the meta-(NC), meta-H, ortho-H, and ortho-(NC) positions relative to the NH group, respectively. The structures and energies of the isomers resulting from recombination of an H-atom with radicals **13** and **14** at different ring positions are summarized in Table S7.

density of the respective radicals at the C3 ring position. Recombination of the H-atom at either N3 or N1 of the benzimidazolyl radical would lead to two equivalent isomers, resulting in the back-formation of the precursor 1H-BzIm. However, recombination at C4, C6, or C8 should lead to the formation of 4H-, 6H-, and 8H-, respectively. Indeed, as shown in Sections 2.2 and 2.3, 4H- and 6H- are two new prototropic tautomers of benzimidazole which were generated photochemically and successfully identified in this work for the first time.

The mere fact of existence as a local minimum on a PES does not guarantee, by itself, a successful capture of a molecular species or its subsequent characterization by stationary spectroscopy, even under cryogenic and inert conditions. It is especially difficult to stabilize those species that can relax to more stable isomers through reactions involving hydrogen atoms, which are prone to undergo quantum tunneling.⁷⁷ This is the case of 8H-BzIm/9H-BzIm, which must be considered fleeting species due to *tunneling instability*.⁷⁸ According to computations, a barrier height of 58.15 kJ mol⁻¹ and a width of 1.82 Bohr separates 8H- from the most stable 1H-tautomer (the same applies for the symmetrically equivalent 9H- and 3H-pair of tautomers; see Figure 8). Shall 8H- (9H-) be formed, it will quickly disappear, on the millisecond time scale, back to 1H- (3H-) BzIm through quantum tunneling (see Table S6 for estimations of rate constants). On the other hand, tautomers 4H- and 6H- are located in much deeper wells (Figure 8), and according to

quantum tunneling estimations (Table S6), once formed, they shall remain in the matrix unchanged, as in fact observed. 2H-BzIm, which throughout the experiments was never detected, has a relative stability between that of 8H- and that of 4H- and 6H-. A barrier height of 90.94 kJ mol⁻¹ and a width of 2.48 Bohr separates 2H- from the most stable 1H-tautomer, rendering it an estimated half-life time of 14 h, which should allow its detection in case it is formed. However, the spin density analysis of the benzimidazolyl radical explains why 2H-BzIm shall not be produced: the unpaired spin density at C2 is very low, making recombination of the radical pair at C2 unlikely.

2.6. Mechanistic Analysis of the Ring-Opening Photochemistry. As shown in Section 2.4, the photochemistry of benzimidazole is not limited to the photoequilibrium among tautomers 1H-, (3H-), 4H-, and 6H-. The photoproducts absorbing at 2200–2000 cm⁻¹ must be formed through some other mechanism. One of such mechanisms would be the cleavage of the N1–C2 bond, occurring upon photoexcitation of benzimidazole, giving rise to open-ring photoproducts.⁷⁹ Cleavage of an X1–C2 bond in azoles is not unprecedented.^{35,51} It is, for instance, the main reactive channel in benzoxazole, which upon UV irradiation, undergoes a concerted O1–C2 cleavage and [1,2] H-shift from C2 to O1 to yield the open-ring 2-isocyanophenol.³⁵ By analogy, the photochemistry discussed below will be referred to as *ring-opening photochemistry*.

Scheme 4. Summary of Dominant Concurrent Photochemistries of Monomeric Benzimidazole Isolated in an Argon Matrix at 15 K^a

^aMolecules 12–20 in the left panel (“ring-opening”), with the isocyano groups shown in red, were identified as a family; the two molecules in the right panel (“fixed-ring”) surrounded by rectangles, 22 and 23, were characterized by at least 15 IR bands each. Note color codes for irradiations at different wavelengths. The black dashed arrows correspond to the recombination of the radical pairs.

The concerted H-shift from C2 to N1, along with the N1–C2 bond cleavage, would lead to ICA (see Figure 6). King, Oliver, and Ashfold reported a comprehensive study of the mechanisms of H atom loss in the parent aniline ($C_6H_5NH_2$), using H-atom photofragment translational spectroscopy,⁸⁰ following excitation in the broad range of UV wavelengths ($294 \text{ nm} > \lambda_{\text{phot}} > 193 \text{ nm}$), accompanied with formation of the aniliny radical in the ground electronic state. Furthermore, the electronic origin of the S_1 excitation in 2-cyanoaniline (the cyano isomer of 12) was reported at $31270 \text{ cm}^{-1} = 319.8 \text{ nm}$ ⁸¹ or at $31265 \pm 2 \text{ cm}^{-1}$.⁸² Therefore, it is likely that also ICA 12 should absorb and undergo NH bond fission at irradiation wavelengths such as 277 nm (or shorter) used in this work to excite BzIm. Hence, the corresponding 2-isocyanoaniliny radical (*syn* 13 and *anti* 14, see Chart 2) should, accordingly, be generated in the matrix, along with an H atom. NBO analysis of the corresponding 2-isocyanoaniliny radicals 13 and 14 revealed that the largest spin density is located at the N1, C5 (*para*), C7 (*ortho*-H), and C9 (*ortho*-NC) atoms (Figure S8), and the NRT analysis corroborated such interpretation (Figure S5). Recombination of the radical pair at the nitrogen atom would lead back to ICA 12, while recombination at the ring carbon atoms would yield its imino isomers 15–20 (see Chart 2). These tautomers are located in deep PES wells, separated from other forms by high barriers (over 170 kJ mol^{-1} , Figure 9). The tautomers with the H atom attached in *meta* position relative to the imino group must be metastable and relax to the more stable neighboring *ortho*- or *para*-isomers through barriers as low as 20 kJ mol^{-1} (Figure 9).

The IR signatures of imino tautomers 17 and 18 with a labile H-atom attached at the *ortho*-(H) position (C atom bearing the H atom) and tautomers 15 and 16 at the *para*-position seem to be the most consistent with the IR signature of the irradiated matrix (see Figure 5). These are the most stable imino tautomers of ICA, having relative energies near $120\text{--}140 \text{ kJ mol}^{-1}$ (see Table S7). Notice the similarity between the amino–imino tautomerism reported herein and the hydroxy–oxo tautomerism reported elsewhere. Namely, there is a direct analogy of the present case with previous observations of the UV-induced photochemistry of substituted

phenols, where the H-atom detached from the OH group recombined precisely at *ortho*-(H) and *para*-positions of the ring, yielding the carbonyl ($C=O$) isomers or their derivatives.^{50,54}

It is also interesting to compare approximate amounts of the photoproducts formed in the two main photochemical pathways of BzIm. The band in the $2140\text{--}2100 \text{ cm}^{-1}$ range was integrated and then normalized by the average value of the computed IR intensities of the $\nu(-N\equiv C)$ mode of photoproducts 12–18. Likewise, the characteristic bands at 1560 cm^{-1} (4H), 1548 cm^{-1} (6H), and $1054/1052 \text{ cm}^{-1}$ (4H + 6H) were integrated and subsequently normalized by the respective computed IR intensities of the 4H and 6H tautomers. According to the analysis of the normalized integrated intensities, we concluded that the ring-open *versus* fixed-ring photoproducted isomers of benzimidazole, corresponding to the two photochemical pathways (Scheme 4), are generated in approximately equal amounts.

3. CONCLUSIONS

The UV-induced photochemistry of monomeric benzimidazole 11 isolated in an argon matrix at 15 K was discovered here to occur *via* two distinct mechanisms with similar yields. The fixed-ring reactivity initiated by irradiations at $\lambda < 280 \text{ nm}$ was characterized by detachment of the labile H atom from the endocyclic NH bond of 1H-BzIm, leading to the intermediacy of the benzimidazolyl radical 21 plus H-atom radical pair, which promptly recombined to yield tautomers 4H- (22) and 6H- (23), as shown in Scheme 4 (right). The characterization of hitherto unobserved tautomers 4H- and 6H- was achieved through their selective consumption by irradiations at $\lambda = 330$ and 283 nm , respectively. Indirect proof of intermediacy by radical 21 is given by NBO analysis, which places most of the spin density on N3 (+0.41), C4 (+0.28), and C6 (+0.29) atoms. Concomitantly, the initial irradiations at $\lambda < 280 \text{ nm}$ led to the formation of a family of compounds bearing the isocyano functional group, namely, ICA 12, which is formed by ring opening of the imidazole moiety coupled with an H-shift from C2 to N1 and also the products of its chemistry 13–18 (see Scheme 4, left).

Interestingly, the photochemistry of monomeric benzimidazole bears no resemblance to its photochemistry in condensed phases^{24,25} but instead has a dual character in contrast to the photochemistry of indole (exclusively fixed-ring) and benzoxazole (exclusively ring-opening),^{35,36} with both of which it shares structural similarities (Chart 1). The observations reported here establish a direct correlation between structural aspects and chemical reactivity and show that neither of the two competitive pathways is surpassed but rather that both co-exist in benzimidazole.

4. EXPERIMENTAL SECTION

Benzimidazole (**1**) was acquired commercially from Alfa Aesar (99% purity). The sample of benzimidazole was placed in a home-made oven that was then connected to a closed-cycle helium cryostat (Advanced Research Systems, DE-202 expander). The sample was purified from volatile impurities by pumping through the cryostat at room temperature using a turbomolecular pump. Monomeric matrices were prepared by allowing the co-deposition of sublimated benzimidazole, whose vapor pressure was thermally enhanced in the oven, and a large excess of argon gas (N60, Air Liquide) onto a cryogenic CsI optical window ($T = 15$ K). The temperature of the CsI window was measured directly using a silicon diode sensor, connected to a digital controller (Scientific Instruments, model 9650-1), and stabilized with an accuracy of 0.1 K.

IR spectra were recorded using a Thermo Nicolet 6700 Fourier-transform IR (FTIR) spectrometer, equipped with a deuterated triglycine sulfate (DTGS) detector and a KBr beam splitter. The spectra were recorded, in the 4000–400 cm^{-1} range, with a resolution of 0.5 cm^{-1} . To avoid interference from atmospheric impurities, a stream of dry and CO_2 filtered-off air was continuously purged through the optical path of the spectrometer.

Ultraviolet (UV) irradiations were performed using a frequency-tunable narrowband pulsed light [full width at half-maximum (fwhm) of 0.2 cm^{-1} , pulse energy ~ 1 mJ], provided by a frequency-doubled signal beam of an optical parametric oscillator (Spectra Physics Quanta-Ray MOPO-SL) pumped using a pulsed Nd:YAG laser (Spectra Physics PRO-230: output power 4.3 W; pulse duration = 10 ns; repetition rate = 10 Hz). The matrices were irradiated through an outer quartz window of the cryostat, and after each irradiation, the transformations were monitored by collecting IR spectra.

5. COMPUTATIONAL SECTION

Geometry optimizations and harmonic frequencies and IR intensities of BzIm and the putative photoproducts were computed at the B97-1/def2-TZVP level of theory^{83,84} using the default parameters of the GAMESS software package.⁸⁵ The method was chosen due to its accuracy at predicting IR spectra of small organic molecules, as shown in a benchmark study of Kesharwani *et al.*⁸⁶ The absolute computed energies of the optimized structures are listed in Table S8, and the respective Cartesian coordinates are collected in Table S9. The nature of each stationary point (as a minimum or a first-order transition state) was inspected by the analysis of its Hessian matrix. The harmonic vibrational frequencies computed at the B97-1/def2-TZVP level for 1H-BzIm were subjected to least-squares linear fit against the experimental frequencies (for BzIm monomers isolated in an argon matrix) in the fingerprint (1700–400 cm^{-1}) range, resulting in a scaling factor of 0.983 (see Figure S2a). This factor, in the fingerprint range, was used to scale the harmonic vibrational frequencies for their subsequent comparison with the experimental wavenumbers, to account for the neglected limitations of the implemented methods and basis set. It is also interesting to note that another method typically used for computational purposes in the

previous studies of our group, B3LYP/6-311++G(d,p), gives exactly the same scaling factor of 0.983 (see Figure S2b) in this spectral range.^{35,54} The harmonic vibrational frequencies in the 3500–2800 and 2300–2000 cm^{-1} ranges were scaled by factors of 0.955 and 0.974, respectively, derived in our previous work for structurally similar compounds (BzOx, 2-isocyanophenol, and 2-cyanophenol).³⁵ The scaled harmonic wavenumbers and absolute IR intensities were used to simulate theoretical IR spectra, by convoluting each peak with a Lorentzian function having an fwhm of 1 cm^{-1} , using the Chemcraft 1.8 software package.⁸⁷ Anharmonic vibrational computations for BzIm were carried out at the B97-1/def2-TZVP level of theory, using the fully automated second-order vibrational perturbation theory (VPT2) approach of Barone *et al.*^{88–90} as defined in the Gaussian 16 (G16) software package.⁹¹ The G16 computations were performed using tight optimization criteria, the ultrafine integration DFT grid, and the integral accuracy threshold enhanced by 2 orders of magnitude. The frequencies of computed anharmonic modes were not scaled.

In addition to the B97-1 method⁸³ and def2-TZVP basis set,⁸⁴ several other model chemistries were used in this study: B3LYP,^{92–94} O3LYP,^{93–95} TPSSH,^{96,97} and B2PLYP⁹⁸ methods combined with the aug-cc-pVTZ,⁹⁹ 6-311++G-(3df,3pd),^{100,101} and 6-311++G(d,p)^{100,101} basis sets. We chose these model chemistries because they proved to be the best choices in our previous studies.^{102,103} All possible combinations of the above-mentioned five methods and four basis sets (20 in total) were used for benchmarking computations. Benchmarking data are organized as a collection of frames in six spectral ranges and are included in the Supporting Information (Figure S10). By comparing results of these computations with the experiment, we found that the B97-1/def2-TZVP and B3LYP/6-311++G(d,p) model chemistries, from the viewpoint of the present study, both perform reliably and are comparable (see Figure S2 for the comparison of the scaling procedure). We selected the B97-1/def2-TZVP method to implement throughout this work.

The electronic structures of the radicals generated in the course of photochemistry of BzIm (closed-ring benzimidazolyl and 2-isocyananiliny radicals) were characterized in detail by the analyses of their natural bond orbitals (NBOs) using the NBO 6.0 software package.¹⁰⁴ Vertical excitation energies of the low-energy electronic excited states were computed using TD-DFT.¹⁰⁵ The results of these calculations are provided in Table S5 of the Supporting Information. The theoretical UV spectra (Figure S3) were simulated using Lorentzian profiles centered at the computed transition wavelengths with a Lorentzian function having a half-width at half-maximum (hwhm) of 0.124 eV (1000 cm^{-1}), as in our previous studies.³⁵

The theoretical normal modes of BzIm were analyzed by carrying out potential energy distribution (PED) analysis. The computed force constants with respect to Cartesian coordinates were transformed into the force constants with respect to internal coordinates, which allowed the PED analysis to be carried out as described elsewhere.¹⁰⁶ The set of internal coordinates used for BzIm was defined as recommended by Pulay *et al.*¹⁰⁷ and is given in Table S1. The atom numbering of BzIm, used for the definition of the internal coordinates, is shown in Figure S1. Marvin software, version 22.15, from ChemAxon, was used for drawing chemical structures, substructures, and reactions.¹⁰⁸

The PESs along the rotamerization and tautomerization reaction paths were computed at the B97-1/def2-TZVP level by following the intrinsic reaction coordinate (IRC) in both directions. For tunneling computations, we used the potential energy profiles along the IRC, computed in non-mass-weighted Cartesian coordinates expressed in units of Bohr. The transmission coefficients of the H-atom tunneling through a parabolic barrier¹⁰⁹ were estimated using the Wentzel–Kramers–Brillouin approximation.^{110–112}

■ ASSOCIATED CONTENT

Data Availability Statement

Data Availability: The data underlying this study are available in the published article and its [Supporting Information](#).

SI Supporting Information

The Supporting Information is available free of charge at <https://pubs.acs.org/doi/10.1021/acs.joc.2c02560>.

Least-squares linear fits of IR spectra computed at the B97-1/def2-TZVP and B3LYP/6-311++G(d,p) levels for 1*H*-tautomer versus experimental IR spectrum of BzIm isolated in an Ar matrix at 15 K; normal mode analysis and vibrational assignments of 1*H*-BzIm, 4*H*-BzIm, and 6*H*-BzIm tautomers; vertical excitation energies, oscillator strengths and simulated UV spectra of 1*H*-, 4*H*-, and 6*H*- tautomers obtained in TD-DFT calculations; experimental and computed IR spectra showing isomerization of 6*H*- into 1*H*- and 4*H*- tautomers upon UV irradiation at 283 nm; predominant resonance structures of the 1*H*-benzimidazole, benzimidazolyl radical, and 2-isocyanoaniliny radical resulting from NRT analysis; computed IRC profiles for the ring-closure reaction of imino-nitrile-ylide to 1*H*-benzimidazole; experimental spectra of UV-irradiated benzimidazole in the 2180–1930 cm⁻¹ range and computed IR spectra of putative photoproducts; computed energies of the isomers on the minor ring-opening pathway of benzimidazole, leading from nitrile-ylide, *via* spiroazirine and triplet vinyl-nitrene, to ketenimine; natural bond orders and natural spin densities computed for anti- and syn-isomers of the 2-isocyanoaniliny radical; IRC profiles for the H-shifts between neighboring heavy atoms in the 2-isocyanoaniliny radical; reaction rates for H-atom tunneling in the closed-ring tautomers of BzIm; Cartesian coordinates and energies computed for all isomers of benzimidazole discussed in this work; comparison of computed IR spectra of 1*H*-BzIm (20 model chemistries: 5 methods × 4 basis sets) with the experimental IR spectrum of benzimidazole monomers isolated in an Ar matrix, shown in six spectral ranges; and selected bibliography reporting on multiple medicinal and pharmaceutical applications of benzimidazole and its vibrational characterization (complementary to the collection of references in the main text) ([PDF](#))

■ AUTHOR INFORMATION

Corresponding Author

Igor Reva – CQC-IMS, Department of Chemistry, University of Coimbra, Coimbra 3004-535, Portugal; CIEPQPF, Department of Chemical Engineering, University of Coimbra, Coimbra 3030-790, Portugal; orcid.org/0000-0001-5983-7743; Email: reva@eq.uc.pt

Authors

José P. L. Roque – CQC-IMS, Department of Chemistry, University of Coimbra, Coimbra 3004-535, Portugal; orcid.org/0000-0002-7845-9415

Mário T. S. Rosado – CQC-IMS, Department of Chemistry, University of Coimbra, Coimbra 3004-535, Portugal; orcid.org/0000-0001-5782-8819

Rui Fausto – CQC-IMS, Department of Chemistry, University of Coimbra, Coimbra 3004-535, Portugal; orcid.org/0000-0002-8264-6854

Complete contact information is available at:

<https://pubs.acs.org/10.1021/acs.joc.2c02560>

Notes

The authors declare no competing financial interest.

■ ACKNOWLEDGMENTS

This work was supported by the project PTDC/QUI-QFI/1880/2020, funded by the Portuguese Science Foundation (“Fundação para a Ciência e a Tecnologia”, FCT). The Coimbra Chemistry Centre (CQC-IMS) is financially supported by FCT, projects UI0313B/00313/2020 and UI0313P/00313/2020, and the Chemical Process Engineering and Forest Products Research Centre (CIEPQPF) is supported by FCT through projects UIDB/EQU/00102/2020 and UIDP/EQU/00102/2020 (National Funds). J.P.L.R. acknowledges FCT for a PhD grant (SFRH/BD/04467/2020).

■ REFERENCES

- (1) Woolley, D. W. Some biological effects produced by benzimidazole and their reversal by purines. *J. Biol. Chem.* **1944**, *152*, 225–232.
- (2) Fischer, O.; Rigaud, M. Ueber Benzimidazole. *Ber. Dtsch. Chem. Ges.* **1902**, *35*, 1258–1265.
- (3) Fischer, O.; Limmer, F. Über Benzimidazole und deren Aufspaltung. *J. Prakt. Chem.* **1906**, *74*, 57–73.
- (4) Fischer, O. Über die Tautomeriefrage bei den Benzimidazolen. *J. Prakt. Chem.* **1907**, *75*, 88–93.
- (5) Saxena, A.; Hegde, V.; Mutalikdesai, S.; Maste, M. Versatility of Benzimidazole and Its Derivatives; an Insight. *Int. J. Pharm. Sci. Res.* **2020**, *11*, 4152–4173.
- (6) Choudhary, S.; Arora, M.; Verma, H.; Kumar, M.; Silakari, O. Benzimidazole based hybrids against complex diseases: A catalogue of the SAR profile. *Eur. J. Pharmacol.* **2021**, *899*, 174027.
- (7) Boiani, M.; González, M. Imidazole and benzimidazole derivatives as chemotherapeutic agents. *Mini-Rev. Med. Chem.* **2005**, *5*, 409–424.
- (8) Bansal, Y.; Silakari, O. The therapeutic journey of benzimidazoles: A review. *Bioorg. Med. Chem.* **2012**, *20*, 6208–6236.
- (9) Shah, K.; Chhabra, S.; Shrivastava, S. K.; Mishra, P. Benzimidazole: a promising pharmacophore. *Med. Chem. Res.* **2013**, *22*, 5077–5104.
- (10) Keri, R. S.; Hiremathad, A.; Budagumpi, S.; Nagaraja, B. M. Comprehensive Review in Current Developments of Benzimidazole-Based Medicinal Chemistry. *Chem. Biol. Drug Des.* **2015**, *86*, 19–65.
- (11) Yadav, G.; Ganguly, S. Structure activity relationship (SAR) study of benzimidazole scaffold for different biological activities: A mini-review. *Eur. J. Med. Chem.* **2015**, *97*, 419–443.
- (12) Gaba, M.; Mohan, C. Development of drugs based on imidazole and benzimidazole bioactive heterocycles: recent advances and future directions. *Med. Chem. Res.* **2016**, *25*, 173–210.
- (13) Akhtar, J.; Khan, A. A.; Ali, Z.; Haider, R.; Shahar Yar, M. S. Structure-activity relationship (SAR) study and design strategies of nitrogen-containing heterocyclic moieties for their anticancer activities. *Eur. J. Med. Chem.* **2017**, *125*, 143–189.

- (14) Akhtar, W.; Khan, M. F.; Verma, G.; Shaquiquzzaman, M.; Rizvi, M. A.; Mehdi, S. H.; Akhter, M.; Alam, M. M. Therapeutic evolution of benzimidazole derivatives in the last quinquennial period. *Eur. J. Med. Chem.* **2017**, *126*, 705–753.
- (15) Beltran-Hortelano, I.; Alcolea, V.; Font, M.; Pérez-Silanes, S. The role of imidazole and benzimidazole heterocycles in Chagas disease: A review. *Eur. J. Med. Chem.* **2020**, *206*, 112692.
- (16) Law, C. S. W.; Yeong, K. Y. Benzimidazoles in Drug Discovery: A Patent Review. *ChemMedChem* **2021**, *16*, 1861–1877.
- (17) López, D. A.; Simison, S. N.; de Sánchez, S. R. The influence of steel microstructure on CO₂ corrosion. EIS studies on the inhibition efficiency of benzimidazole. *Electrochim. Acta* **2003**, *48*, 845–854.
- (18) Aljourani, J.; Raeissi, K.; Golozar, M. A. Benzimidazole and its derivatives as corrosion inhibitors for mild steel in 1M HCl solution. *Corrosion Sci.* **2009**, *51*, 1836–1843.
- (19) Obot, I. B.; Edouk, U. M. Benzimidazole: Small planar molecule with diverse anti-corrosion potentials. *J. Mol. Liq.* **2017**, *246*, 66–90.
- (20) Marinescu, M. Recent advances in the use of benzimidazoles as corrosion inhibitors. *BMC Chem.* **2019**, *13*, 136.
- (21) Mishra, A.; Aslam, J.; Verma, C.; Quraishi, M. A.; Ebenso, E. E. Imidazoles as highly effective heterocyclic corrosion inhibitors for metals and alloys in aqueous electrolytes: A review. *J. Taiwan Inst. Chem. Eng.* **2020**, *114*, 341–358.
- (22) Goni, L. K. M. O.; Jafar Mazumder, M. A. J.; Quraishi, M. A.; Mizanur Rahman, M. M. Bioinspired Heterocyclic Compounds as Corrosion Inhibitors: A Comprehensive Review. *Chem. Asian J.* **2021**, *16*, 1324–1364.
- (23) Horak, E.; Kassal, P.; Murković Steinberg, I. Benzimidazole as a structural unit in fluorescent chemical sensors: the hidden properties of a multifunctional heterocyclic scaffold. *Supramol. Chem.* **2018**, *30*, 838–857.
- (24) Cole, E. R.; Crank, G.; Lye, E. Photochemistry of Heterocyclics. II. Photolysis of Benzimidazole and its 2-Alkyl Derivatives. *Aust. J. Chem.* **1978**, *31*, 2675–2684.
- (25) Smitka, J.; Lemos, A.; Porel, M.; Jockusch, S.; Belderrain, T. R.; Tesárová, E.; Da Silva, J. P. Phototransformation of benzimidazole and thiabendazole inside cucurbit[8]uril. *Photochem. Photobiol. Sci.* **2014**, *13*, 310–315.
- (26) O'Connell, J. M.; Moriarty, E.; Aldabbagh, F. Access to Aromatic Ring-Fused Benzimidazoles Using Photochemical Substitutions of the Benzimidazol-2-yl Radical. *Synthesis* **2012**, *44*, 3371–3377.
- (27) Tiefenthaler, H.; Dörscheln, W.; Göth, H.; Schmid, H. Photoisomerisation von Indazolen zu Benzimidazolen. *Tetrahedron Lett.* **1964**, *5*, 2999–3001.
- (28) Tiefenthaler, H.; Dörscheln, W.; Göth, H.; Schmid, H. Photoisomerisierung von Pyrazolen und Indazolen zu Imidazolen bzw. Benzimidazolen und 2-Amino-benzonitrilen. *Helv. Chim. Acta* **1967**, *50*, 2244–2258.
- (29) Lefebvre, C.; Fortier, L.; Hoffmann, N. Photochemical Rearrangements in Heterocyclic Chemistry. *Eur. J. Org. Chem.* **2020**, *2020*, 1393–1404.
- (30) Heinzelmann, W.; Märky, M.; Gilgen, P. Zum Mechanismus der photochemischen Umwandlung von 2-Alkyl-indazolen in 1-Alkyl-benzimidazole. I. Struktur und Reaktivität eines Zwischenproduktes. *Helv. Chim. Acta* **1976**, *59*, 1512–1527.
- (31) Heinzelmann, W.; Märky, M.; Gilgen, P. Zum Mechanismus der photochemischen Umwandlung von 2-Alkyl-indazolen in 1-Alkyl-benzimidazole. II. Photophysikalische und photochemische Primärprozesse. *Helv. Chim. Acta* **1976**, *59*, 1528–1546.
- (32) Heinzelmann, W.; Märky, M.; Gilgen, P. Zum Mechanismus der Photochemie von 2-Alkylindazolen in wässrigen Lösungen. *Helv. Chim. Acta* **1976**, *59*, 2362–2373.
- (33) Nigam, S.; Dogra, S. K. Proton Transfer Reactions of Benzimidazole in Ionic Micelles in the Excited Singlet State. *J. Photochem. Photobiol., A* **1990**, *54*, 219–230.
- (34) Roque, J. P. L.; Nunes, C. M.; Fausto, R. Matrix Isolation in Heterocyclic Chemistry. In *Heterocycles: Synthesis, Catalysis, Sustainability, and Characterization*; Pinho e Melo, T. M. V. D., Pineiro, M., Eds.; John Wiley & Sons, Ltd., 2022; Chapter 12, pp 401–451.
- (35) Reva, I.; Lopes Jesus, A. J.; Nunes, C. M.; Roque, J. P. L.; Fausto, R. UV-Induced Photochemistry of 1,3-Benzoxazole, 2-Isocyanophenol, and 2-Cyanophenol Isolated in Low-Temperature Ar Matrixes. *J. Org. Chem.* **2021**, *86*, 6126–6137.
- (36) Reva, I.; Lapinski, L.; Lopes Jesus, A. J.; Nowak, M. J. Photoinduced transformations of indole and 3-formylindole monomers isolated in low-temperature matrices. *J. Chem. Phys.* **2017**, *147*, 194304.
- (37) Nowak, M. J.; Reva, I.; Rostkowska, H.; Lapinski, L. UV-induced hydrogen-atom transfer and hydrogen-atom detachment in monomeric 7-azaindole isolated in Ar and n-H₂ matrices. *Phys. Chem. Chem. Phys.* **2017**, *19*, 11447–11454.
- (38) Klots, T. D.; Devlin, P.; Collier, W. B. Heteroatom derivatives of indene V. Vibrational spectra of benzimidazole. *Spectrochim. Acta, Part A* **1997**, *53*, 2445–2456.
- (39) Velino, B.; Trombetti, A.; Canè, E.; Corbelli, G.; Caminati, W. Microwave Spectrum of Benzimidazole. *J. Mol. Spectrosc.* **1992**, *152*, 434–440.
- (40) Berden, G.; Meerts, W. L.; Jalviste, E. Rotationally Resolved Ultraviolet Spectroscopy of Indole, Indazole, and Benzimidazole: Inertial Axis Reorientation in the S₁(¹L_b)←S₀ Transitions. *J. Chem. Phys.* **1995**, *103*, 9596–9606.
- (41) Schmitt, M.; Krügler, D.; Böhm, M.; Rätzer, C.; Bednarska, V.; Kalkman, I.; Leo Meerts, W. L. A genetic algorithm based determination of the ground and excited (¹L_b) state structure and the orientation of the transition dipole moment of benzimidazole. *Phys. Chem. Chem. Phys.* **2006**, *8*, 228–235.
- (42) Jalviste, E.; Treshchalov, A. Spectroscopy of Jet-Cooled Benzimidazole and Benzotriazole. *Chem. Phys.* **1993**, *172*, 325–338.
- (43) Jacoby, C.; Roth, W.; Schmitt, M. A comparison of intermolecular vibrations and tautomerism in benzimidazole, benzotriazole and their binary water clusters. *Appl. Phys. B: Lasers Opt.* **2000**, *71*, 643–649.
- (44) Schoone, K.; Smets, J.; Houben, L.; Van Bael, M. K.; Adamowicz, L.; Maes, G. Matrix-isolation FT-IR studies and theoretical calculations of hydrogen-bonded complexes of molecules modeling adenine tautomers. I. H-bonding of benzimidazoles with H₂O in Ar matrices. *J. Phys. Chem. A* **1998**, *102*, 4863–4877.
- (45) Gordon, R. D.; Chan, W. H. W. Origin Band Shifts Upon Deuteration in the 280 nm Absorption System of Benzimidazole. *Spectrosc. Lett.* **1977**, *10*, 571–586.
- (46) Gordon, R. D.; Yang, R. F. Vapor Absorption Spectra of Benzoxazole, Benzimidazole, and Benzothiazole near 2850 Å. *Can. J. Chem.* **1970**, *48*, 1722–1729.
- (47) Lin, J. L.; Li, Y. C.; Tzeng, W. B. Mass analyzed threshold ionization spectroscopy of aza-aromatic bicyclic molecules: Benzimidazole and benzotriazole. *Chem. Phys.* **2007**, *334*, 189–195.
- (48) Maki, I.; Nishimoto, K.; Sugiyama, M.; Hiratsuka, H.; Tanizaki, Y. Polarized Absorption Spectra of Indole and Benzimidazole. *Bull. Chem. Soc. Jpn.* **1981**, *54*, 8–12.
- (49) It should be noted here that the 4*H*-BzIm and 6*H*-BzIm are symmetry-equivalent isomers of 7*H*-BzIm and 5*H*-BzIm, respectively (as can be noted in Table 1). The reason for choice of 4*H*- and 6*H*-isomers, over the other two counterparts, is related with the positions of the highest spin density in the benzimidazolyl radical, as discussed in Section 2.5.
- (50) Reva, I.; Nowak, M. J.; Lapinski, L.; Fausto, R. Hydrogen atom transfer reactions in thiophenol: photogeneration of two new thione isomers. *Phys. Chem. Chem. Phys.* **2015**, *17*, 4888–4898.
- (51) Miyazaki, J.; Takiyama, H.; Nakata, M. Isocyanate compounds newly recognized in photochemical reaction of thiazole: matrix-isolation FT-IR and theoretical studies. *RSC Adv.* **2017**, *7*, 4960–4974.
- (52) Bernstein, M. P.; Sandford, S. A.; Allamandola, L. J. The infrared spectra of nitriles and related compounds frozen in Ar and H₂O. *Astrophys. J.* **1997**, *476*, 932–942.

- (53) You, M.; Zhou, L.; Huang, X.; Wang, Y.; Zhang, W. Isonitrile-Derivatized Indole as an Infrared Probe for Hydrogen-Bonding Environments. *Molecules* **2019**, *24*, 1379.
- (54) Lopes Jesus, A. J.; Reva, I.; Nunes, C. M.; Roque, J. P. L.; Pinto, S. M. V.; Fausto, R. Kinetically unstable 2-isocyanophenol isolated in cryogenic matrices: Vibrational excitation, conformational changes and spontaneous tunneling. *Chem. Phys. Lett.* **2020**, *747*, 137069.
- (55) Maj, M.; Ahn, C.; Blasiak, B.; Kwak, K.; Han, H.; Cho, M. Isonitrile as an Ultrasensitive Infrared Reporter of Hydrogen-Bonding Structure and Dynamics. *J. Phys. Chem. B* **2016**, *120*, 10167–10180.
- (56) Gée, C.; Douin, S.; Crépin, C.; Bréchnignac, P. Infrared spectroscopy of aniline ($C_6H_5NH_2$) and its cation in a cryogenic argon matrix. *Chem. Phys. Lett.* **2001**, *338*, 130–136.
- (57) Kawamata, K.; Chowdhury, P. K.; Ito, F.; Sugawara, K.; Nakanaga, T. Investigation of the N–H stretching vibrations of the aniline–pyrrole binary complex and its cation by infrared depletion spectroscopy. *J. Phys. Chem. A* **1998**, *102*, 4788–4793.
- (58) Mukherjee, M.; Bandyopadhyay, B.; Biswas, P.; Chakraborty, T. Amine inversion effects on the IR spectra of aniline in the gas phase and cold inert gas matrixes. *Indian J. Phys.* **2012**, *86*, 201–208.
- (59) Nakanaga, T.; Ito, F.; Miyawaki, J.; Sugawara, K.; Takeo, H. Observation of the infrared spectra of the NH_2 -stretching vibration modes of aniline– Ar_n ($n = 1,2$) clusters in a supersonic jet using REMPI. *Chem. Phys. Lett.* **1996**, *261*, 414–420.
- (60) Honda, M.; Fujii, A.; Fujimaki, E.; Ebata, T.; Mikami, N. NH stretching vibrations of jet-cooled aniline and its derivatives in the neutral and cationic ground states. *J. Phys. Chem. A* **2003**, *107*, 3678–3686.
- (61) Nalepa, R. A.; Lapos, J. D. Vibrational Spectra of Phenylisocyanide and Perdeutero-phenylisocyanide. *J. Mol. Spectrosc.* **1974**, *50*, 106–114.
- (62) Recombination of the H atom with 13 or 14 at meta position (with respect to the NH group) is unlikely as explained in Section 2.6.
- (63) Sobolewski, A. L.; Domcke, W.; Dedonder-Lardeux, C.; Jouvét, C. Excited-state hydrogen detachment and hydrogen transfer driven by repulsive $^1\pi\sigma^*$ states: A new paradigm for nonradiative decay in aromatic biomolecules. *Phys. Chem. Chem. Phys.* **2002**, *4*, 1093–1100.
- (64) Ashfold, M. N. R.; King, G. A.; Murdock, D.; Nix, M. G. D.; Oliver, T. A. A.; Sage, A. G. $\pi\sigma^*$ excited states in molecular photochemistry. *Phys. Chem. Chem. Phys.* **2010**, *12*, 1218–1238.
- (65) Cronin, B.; Nix, M. G. D.; Qadiri, R. H.; Ashfold, M. N. R. High resolution photofragment translational spectroscopy studies of the near ultraviolet photolysis of pyrrole. *Phys. Chem. Chem. Phys.* **2004**, *6*, 5031–5041.
- (66) Nix, M. G. D.; Devine, A. L.; Cronin, B.; Ashfold, M. N. R. High resolution photofragment translational spectroscopy of the near UV photolysis of indole: Dissociation via the $^1\pi\sigma^*$ state. *Phys. Chem. Chem. Phys.* **2006**, *8*, 2610–2618.
- (67) Nix, M. G. D.; Devine, A. L.; Cronin, B.; Ashfold, M. N. R. Ultraviolet photolysis of adenine: Dissociation via the $^1\pi\sigma^*$ state. *J. Chem. Phys.* **2007**, *126*, 124312.
- (68) Ashfold, M. N. R.; Cronin, B.; Devine, A. L.; Dixon, R. N.; Nix, M. G. D. The role of $\pi\sigma^*$ excited states in the photodissociation of heteroaromatic molecules. *Science* **2006**, *312*, 1637–1640.
- (69) Barbatti, M.; Lischka, H.; Salzmann, S.; Marian, C. M. UV excitation and radiationless deactivation of imidazole. *J. Chem. Phys.* **2009**, *130*, 034305.
- (70) King, G. A.; Oliver, T. A. A.; Nix, M. G. D.; Ashfold, M. N. R. Exploring the mechanisms of H atom loss in simple azoles: Ultraviolet photolysis of pyrazole and triazole. *J. Chem. Phys.* **2010**, *132*, 064305.
- (71) Crespo-Otero, R.; Barbatti, M.; Yu, H.; Evans, N. L.; Ullrich, S. Ultrafast Dynamics of UV-Excited Imidazole. *ChemPhysChem* **2011**, *12*, 3365–3375.
- (72) Iizumi, S.; Ninomiya, S.; Sekine, M.; Nakata, M. First observation of infrared and UV-visible absorption spectra of adenine radical in low-temperature argon matrices. *J. Mol. Struct.* **2012**, *1025*, 43–47.
- (73) Lopes Jesus, A. J.; Reva, I.; Fausto, R. UV-induced transformations in matrix-isolated 6-methoxyindole. *J. Photochem. Photobiol., A* **2017**, *336*, 123–130.
- (74) Lopes Jesus, A. J.; Rosado, M. T. S.; Fausto, R.; Reva, I. UV-induced radical formation and isomerization of 4-methoxyindole and 5-methoxyindole. *Phys. Chem. Chem. Phys.* **2020**, *22*, 22943–22955.
- (75) Chmura, B.; Rode, M. F.; Sobolewski, A. L.; Lapinski, L.; Nowak, M. J. A Computational Study on the Mechanism of Intramolecular Oxo-Hydroxy Phototautomerism Driven by Repulsive $\pi\sigma^*$ State. *J. Phys. Chem. A* **2008**, *112*, 13655–13661.
- (76) Sobolewski, A. L.; Adamowicz, L. An ab initio study of the potential energy surface in the S_1 state of 2-hydroxypyridine. *Chem. Phys.* **1996**, *213*, 193–201.
- (77) Halasa, A.; Lapinski, L.; Reva, I.; Rostkowska, H.; Fausto, R.; Nowak, M. J. Near-Infrared Laser-Induced Generation of Three Rare Conformers of Glycolic Acid. *J. Phys. Chem. A* **2014**, *118*, 5626–5635.
- (78) Amlani, H.; Frenklah, A.; Kozuch, S. Tunneling Instability in Molecular Systems. An Exercise in Computational Chemistry Prediction Power. In *Tunneling in Molecules: Nuclear Quantum Effects from Bio to Physical Chemistry*; Kästner, J., Kozuch, S., Eds.; The Royal Society of Chemistry, 2020; Chapter 2, pp 61–87.
- (79) Just like in benzoxazole, the sole cleavage of the N1–C2 bond in benzimidazole would lead to a fleeting nitrile ylide species. In the course of this study we verified this hypothesis and confirmed that in the present experiment this reaction channel accounts for no more than 1–2% of all observed photo transformations. See a more detailed discussion of this subject in the [Supporting Information](#).
- (80) King, G. A.; Oliver, T. A. A.; Ashfold, M. N. R. Dynamical insights into $^1\pi\sigma^*$ state mediated photodissociation of aniline. *J. Chem. Phys.* **2010**, *132*, 214307.
- (81) Kolek, P.; Pirowska, K.; Najbar, J. LIF excitation spectra of *o*- and *m*-cyanoanilines. *Phys. Chem. Chem. Phys.* **2001**, *3*, 4874–4888.
- (82) Jin, Y. H.; Zhao, Y.; Yang, Y. G.; Wang, L. R.; Li, C. Y.; Jia, S. T. Two-color resonance enhanced multi-photon ionization and mass analyzed threshold ionization spectroscopy of 2-aminobenzonitrile and the CN substitution effect. *Chem. Phys. Lett.* **2018**, *692*, 395–401.
- (83) Hamprecht, F. A.; Cohen, A. J.; Tozer, D. J.; Handy, N. C. Development and assessment of new exchange-correlation functionals. *J. Chem. Phys.* **1998**, *109*, 6264–6271.
- (84) Weigend, F.; Ahlrichs, R. Balanced basis sets of split valence, triple zeta valence and quadruple zeta valence quality for H to Rn: Design and assessment of accuracy. *Phys. Chem. Chem. Phys.* **2005**, *7*, 3297–3305.
- (85) Schmidt, M. W.; Baldridge, K. K.; Boatz, J. A.; Elbert, S. T.; Gordon, M. S.; Jensen, J. H.; Koseki, S.; Matsunaga, N.; Nguyen, K. A.; Su, S.; Windus, T. L.; Dupuis, M.; Montgomery, J. A., Jr. General atomic and molecular electronic structure system. *J. Comput. Chem.* **1993**, *14*, 1347–1363.
- (86) Kesharwani, M. K.; Brauer, B.; Martin, J. M. L. Frequency and Zero-Point Vibrational Energy Scale Factors for Double-Hybrid Density Functionals (and Other Selected Methods): Can Anharmonic Force Fields Be Avoided? *J. Phys. Chem. A* **2015**, *119*, 1701–1714.
- (87) Zhurko, G. A. *Chemcraft—Graphical Program for Visualization of Quantum Chemistry Computations*; version 1.8, 2016. <http://www.chemcraftprog.com>.
- (88) Barone, V.; Bloino, J.; Guido, C. A.; Lipparini, F. A fully automated implementation of VPT2 Infrared intensities. *Chem. Phys. Lett.* **2010**, *496*, 157–161.
- (89) Bloino, J.; Barone, V. A second-order perturbation theory route to vibrational averages and transition properties of molecules: General formulation and application to infrared and vibrational circular dichroism spectroscopies. *J. Chem. Phys.* **2012**, *136*, 124108.
- (90) Barone, V.; Biczysko, M.; Bloino, J. Fully anharmonic IR and Raman spectra of medium-size molecular systems: accuracy and interpretation. *Phys. Chem. Chem. Phys.* **2014**, *16*, 1759–1787.
- (91) Frisch, M. J.; Trucks, G. W.; Schlegel, H. B.; Scuseria, G. E.; Robb, M. A.; Cheeseman, J. R.; Scalmani, G.; Barone, V.; Petersson, G. A.; Nakatsuji, H.; Li, X.; Caricato, M.; Marenich, A. V.; Bloino, J.; Janesko, B. G.; Gomperts, R.; Mennucci, B.; Hratchian, H. P.; Ortiz, J.

V.; Izmaylov, A. F.; Sonnenberg, J. L.; Williams-Young, D.; Ding, F.; Lipparini, F.; Egidi, F.; Goings, J.; Peng, B.; Petrone, A.; Henderson, T.; Ranasinghe, D.; Zakrzewski, V. G.; Gao, J.; Rega, N.; Zheng, G.; Liang, W.; Hada, M.; Ehara, M.; Toyota, K.; Fukuda, R.; Hasegawa, J.; Ishida, M.; Nakajima, T.; Honda, Y.; Kitao, O.; Nakai, H.; Vreven, T.; Throssell, K.; Montgomery, J. A., Jr.; Peralta, J. E.; Ogliaro, F.; Bearpark, M. J.; Heyd, J. J.; Brothers, E. N.; Kudin, K. N.; Staroverov, V. N.; Keith, T. A.; Kobayashi, R.; Normand, J.; Raghavachari, K.; Rendell, A. P.; Burant, J. C.; Iyengar, S. S.; Tomasi, J.; Cossi, M.; Millam, J. M.; Klene, M.; Adamo, C.; Cammi, R.; Ochterski, J. W.; Martin, R. L.; Morokuma, K.; Farkas, O.; Foresman, J. B.; Fox, D. J. *Gaussian 16*; Revision C.01; Gaussian, Inc.: Wallingford, CT, 2016.

(92) Becke, A. D. Density-functional thermochemistry. III. The role of exact exchange. *J. Chem. Phys.* **1993**, *98*, 5648–5652.

(93) Vosko, S. H.; Wilk, L.; Nusair, M. Accurate spin-dependent electron liquid correlation energies for local spin density calculations: a critical analysis. *Can. J. Phys.* **1980**, *58*, 1200–1211.

(94) Lee, C. T.; Yang, W. T.; Parr, R. G. Development of the Colle-Salvetti correlation-energy formula into a functional of the electron density. *Phys. Rev. B* **1988**, *37*, 785–789.

(95) Cohen, A. J.; Handy, N. C. Dynamic Correlation. *Mol. Phys.* **2001**, *99*, 607–615.

(96) Staroverov, V. N.; Scuseria, G. E.; Tao, J. M.; Perdew, J. P. Comparative assessment of a new nonempirical density functional: Molecules and hydrogen-bonded complexes. *J. Chem. Phys.* **2003**, *119*, 12129–12137.

(97) Tao, J. M.; Perdew, J. P.; Staroverov, V. N.; Scuseria, G. E. Climbing the density functional ladder: Nonempirical meta-generalized gradient approximation designed for molecules and solids. *Phys. Rev. Lett.* **2003**, *91*, 146401.

(98) Grimme, S. Semiempirical hybrid density functional with perturbative second-order correlation. *J. Chem. Phys.* **2006**, *124*, 034108.

(99) Kendall, R. A.; Dunning, T. H., Jr.; Harrison, R. J. Electron Affinities of the First-Row Atoms Revisited. Systematic Basis Sets and Wave Functions. *J. Chem. Phys.* **1992**, *96*, 6796–6806.

(100) Krishnan, R.; Binkley, J. S.; Seeger, R.; Pople, J. A. Self-consistent molecular orbital methods. XX. A basis set for correlated wave functions. *J. Chem. Phys.* **1980**, *72*, 650–654.

(101) Frisch, M. J.; Pople, J. A.; Binkley, J. S. Self-consistent molecular orbital methods. 25. Supplementary functions for Gaussian basis sets. *J. Chem. Phys.* **1984**, *80*, 3265–3269.

(102) Duarte, L.; Reva, I.; Cristiano, M. L. S.; Fausto, R. Photoisomerization of Saccharin. *J. Org. Chem.* **2013**, *78*, 3271–3275.

(103) Nunes, C. M.; Reva, I.; Fausto, R. Conformational isomerizations triggered by vibrational excitation of second stretching overtones. *Phys. Chem. Chem. Phys.* **2019**, *21*, 24993–25001.

(104) Glendenning, E. D.; Landis, C. R.; Weinhold, F. NBO 6.0: Natural bond orbital analysis program. *J. Comput. Chem.* **2013**, *34*, 1429–1437.

(105) Bauernschmitt, R.; Ahlrichs, R. Treatment of electronic excitations within the adiabatic approximation of time dependent density functional theory. *Chem. Phys. Lett.* **1996**, *256*, 454–464.

(106) Schachtschneider, J. H.; Mortimer, F. S. *Vibrational Analysis of Polyatomic Molecules VI. FORTRAN IV Programs for Solving the Vibrational Secular Equation and for the Least-Squares Refinement of Force Constants*. Project No. 31450. Structural Interpretation of Spectra; Shell Development Co.: Emeryville, CA, 1969. Technical Report No. 57-65.

(107) Pulay, P.; Fogarasi, G.; Pang, F.; Boggs, J. E. Systematic ab Initio Gradient Calculation of Molecular Geometries, Force Constants, and Dipole Moment Derivatives. *J. Am. Chem. Soc.* **1979**, *101*, 2550–2560.

(108) Cherinka, B.; Andrews, B. H.; Sánchez-Gallego, J.; Brownstein, J.; Argudo-Fernández, M.; Blanton, M.; Bundy, K.; Jones, A.; Masters, K.; Law, D. R.; Rowlands, K.; Weijmans, A. M.; Westfall, K.; Yan, R. B. Marvin: A Tool Kit for Streamlined Access and Visualization of the SDSS-IV MaNGA Data Set. *Astron. J.* **2019**, *158*, 74.

(109) Borden, W. T. Reactions that involve tunneling by carbon and the role that calculations have played in their study. *Wiley Interdiscip. Rev.: Comput. Mol. Sci.* **2016**, *6*, 20–46.

(110) Wentzel, G. Eine Verallgemeinerung der Quantenbedingungen für die Zwecke der Wellenmechanik. *Z. Phys.* **1926**, *38*, 518–529.

(111) Kramers, H. A. Wellenmechanik und halbzahlige Quantisierung. *Z. Phys.* **1926**, *39*, 828–840.

(112) Brillouin, L. La mécanique ondulatoire de Schrödinger; une méthode générale de résolution par approximations successives. *C. R. Hebd. Seances Acad. Sci.* **1926**, *183*, 24–26 <http://gallica.bnf.fr/ark:/12148/bpt6k3136h/f24>.

Recommended by ACS

Photochemistry of 1-(2- and 3-Thienyl)diazoethanes: Spectroscopy and Tunneling Reaction of Triplet 1-(3-Thienyl)ethylidene

Caroline R. Pharr, Robert J. McMahon, *et al.*

NOVEMBER 10, 2023

THE JOURNAL OF ORGANIC CHEMISTRY

READ 

Adamantylidencarbene: Photochemical Generation, Trapping, and Theoretical Studies

Alexander D. Roth, Dasan M. Thamattoor, *et al.*

SEPTEMBER 28, 2023

THE JOURNAL OF ORGANIC CHEMISTRY

READ 

3-Substituted 2-Aminonaphthalene Photocages for Carboxylic Acids and Alcohols; Decaging Mechanism and Potential Applications in Synthesis

Vilma Lovrinčević, Nikola Basarić, *et al.*

OCTOBER 13, 2023

THE JOURNAL OF ORGANIC CHEMISTRY

READ 

Unraveling the Solid-State Photoreactivity of Carbonylbis(4,1-Phenylene)dicarbonazidate with Laser Flash Photolysis

Noha Ahmed, Anna D. Gudmundsdottir, *et al.*

NOVEMBER 08, 2023

THE JOURNAL OF PHYSICAL CHEMISTRY A

READ 

Get More Suggestions >